# Attrition Studies of an Iron Fischer−Tropsch Catalyst Used in a Pilot-Scale Stirred Tank Slurry Reactor

**ARTICLE** *in* INDUSTRIAL & ENGINEERING CHEMISTRY RESEARCH · SEPTEMBER 2012

Impact Factor: 2.59 · DOI: 10.1021/ie3014428



**3 AUTHORS**, INCLUDING:

Tiejun Lin
East China University of Science and Technology
**6** PUBLICATIONS **12** CITATIONS

SEE PROFILE

li Shi
East China University of Science and Technology
**68** PUBLICATIONS **350** CITATIONS

SEE PROFILE

I&EC research
Industrial & Engineering Chemistry Research

Article

pubs.acs.org/IECR

# Attrition Studies of an Iron Fischer–Tropsch Catalyst Used in a Pilot-Scale Stirred Tank Slurry Reactor

Tie-jun Lin, Xuan Meng, and Li Shi*

The State Key Laboratory of Chemical Engineering, East China University of Science and Technology, Shanghai 200237, People's Republic of China

**ABSTRACT:** Attrition resistance is a key design parameter for catalysts used in slurry phase Fischer–Tropsch (F–T) reactors, especially for industrial-scale reaction. It is well-known that iron F–T catalyst particles undergo physical attrition and chemical stresses caused by phase transformations. Here we report on attrition properties of a Fe–Cu–K–$SiO_2$ catalyst used in a pilot-scale stirred tank slurry reactor (STSR) under low temperature F–T reaction conditions. The wax-free catalysts were characterized by SEM, EDS, BET surface area measurements, and a Mastersizer 2000 for particle size analysis. The results show that, after 408 h of reaction in an STSR, the particle size reduction due to erosion/abrasion and fracture was apparent. Large reductions in the Sauter mean diameter (93.45%) and the volume moment diameter (71.67%) were observed. The increase in the fractions of particles smaller than 5 and 10 $\mu$m was 18.25 and 30.11%, respectively. We concluded therefore that the catalyst underwent more severe attrition in industrial application and the attrition was mainly caused by the fracture of larger or smaller particles. Further study is needed to improve the catalyst attrition resistance.

## 1. INTRODUCTION

Attrition, defined as the breakup of catalyst particles, is a commonly encountered troublesome problem in three phase slurry Fischer–Tropsch (F–T) synthesis (slurry bubble column reactor (SBCR) or stirred tank slurry reactor (STSR)), especially for iron F–T catalysts used in industrial-scale reactors.[1] Difficulties with catalyst/wax separation due to the breakdown of the original catalyst particles to fine particles (attrition) occurred during an F–T demonstration run in an SBCR in La Porte, Texas, USA, using a precipitated iron catalyst,[2] and in a commercial scale SBCR at a Qatar Oryx plant using a supported cobalt catalyst.[3,4] It is reported that, after 1 day of operation, the filtering system was seriously plugged, and the settling tank also failed to separate the catalyst/wax efficiently, which resulted in the gradual loss of catalyst, and the plant operated below the design capacity.

The wax/catalyst separation problem has been a major developmental challenge in the commercial application of SBCRs and STSRs for low temperature iron-based F–T synthesis.[5,6] Generation of fine particles would contaminate the product, affect the downstream wax processing, limit the mass and heat transfer due to the increase in viscosity, and even lead to the shutdown of industrial reactors.[7,8] Therfore, more attention should be paid to studying and monitoring the attrition behavior of catalysts used in experimental, pilot-scale, or industrial-scale reactors.

In recent years, many research groups have made a lot of effort to study and improve the attrition resistance of iron F–T catalysts without sacrificing either the activity or the selectivity of these catalysts.[9−11] It is believed that the attrition process of iron catalysts for F–T synthesis includes both fracture (the fragmentation of particles) and abrasion/erosion (the process by which particle surface layers or corners are removed).[1,7] The catalysts undergo various types of stresses during the F–T reaction, such as contact, thermal, pressure, and chemical stresses.[12] In Fischer–Tropsch synthesis, such attrition can also be classified into physical attrition resulting from collision between catalyst particles and the reactor internals and chemical attrition caused by volume changes and carbon deposition that accompany the phase transformation of iron oxide precursor into iron carbide.[9,11] A report stated that conversion of $Fe_3C$ to $Fe_3O_4$ results in an increase in volume of 91%, and a similar increase for $\chi$-$Fe_5C_2$.[13] The volumetric change would cause stress in the catalyst particles which may lead to attrition and formation of small crystallites of iron carbides that split off rapidly to form ultrafine particles.[13] According to the impact velocity, contact geometry, particle size, and particle shape,[1] the particle attrition can be further categorized into different breakage modes. For example, particle fracture due to preexisting internal or surface flaws is classified as brittle failure; crack initiation is considered to be semibrittle failure (fragmentation or chipping depending on the position of the cracks).

According to the literature, many factors such as silica type and concentration, the morphology of primary particles formed during the catalyst synthesis, phase transformation, and carburization during the F–T reaction are important in determining the attrition strength of an iron F–T catalyst.[14,15] Zhao et al.[14] reported that particle density, among all particle properties of the catalysts, correlates with the intrinsic catalyst attrition resistance. To improve the attrition resistance, spray drying is used to prepare microspherical particles, and nearly all the industrial F–T catalysts possess this shape.

The attrition mechanisms in an STSR are still not clear due to the complex nature of attrition; hence it is necessary to develop a suitable evaluation of catalyst resistance. These

**Received:** June 2, 2012
**Revised:** August 26, 2012
**Accepted:** September 13, 2012
**Published:** September 13, 2012





dx.doi.org/10.1021/ie3014428 | *Ind. Eng. Chem. Res.* 2012, 51, 13123–13131

technologies include the following: collision test, ASTM fluidized bed test, jet cup test, ultrasonic tests, rotating drum test, and slurry bed test.[1] However, different test methods generate some slight differences in the results,[16] and the laboratory tests cannot produce exactly the same attrition results as in industrial-scale STSRs. Sometimes a catalyst with high attrition resistance in experimental attrition tests shows weak attrition resistance conversely when used in the scale-up of reactors. Furthermore, there have been only a few studies of attrition behavior in a pilot-scale STSR under reactive conditions. It is much harder to find literature about the continuous recording of the particle size distribution (PSD) and dynamic changes of morphology.

Consequently, the objective of this research is to monitor the particle size distribution and morphological changes of an iron working catalyst during the F−T synthesis in a pilot-scale STSR. The catalyst samples were withdrawn from the same point of the STSR at different times on stream to determine the combined extent of physical and chemical attrition. The extent of attrition was determined by comparing the particle size distributions. The morphologies of catalysts at different reaction times were obtained by use of scanning electron microscopy (SEM). Energy-dispersive X-ray spectroscopy (EDS) was performed to observe the changes of surface elements of catalyst particles. Finally, we try to explain the attrition mechanisms of catalysts in STSRs and incorporate this understanding into the design of iron catalysts with superior attrition resistance and further design and optimize the continuous flow filtration unit for wax/catalyst separation.

## 2. EXPERIMENTAL SECTION

**2.1. Catalyst.** An industrially available iron catalyst designed for 10 000 tons was used to test its attrition behavior in an STSR. The properties reported for the catalyst were average size of 30−200 $\mu$m, surface area of 160−210 $m^2 \cdot g^{-1}$, bulk density of 0.6−0.8 $g \cdot cm^{-3}$, and erosion index measured by jet cup smaller than 7%. Light liquid paraffin was used as the start-up solvent. Details of the catalyst preparation procedure and STSR tests such as the experiment setup, operating procedures, and product quantification can be found elsewhere.

**2.2. Catalyst/Wax Separation.** Catalyst/wax slurry was withdrawn from the same point of the STSR at different times on stream (TOS = 0, 120, 216, 288, 312, 336, 360, 408 h) via the dip tube after sufficient purging with $N_2$. Subsequently, a novel extraction−filtration separator (EFS), see Figure 1, was used to remove wax from F−T wax/catalyst slurry mixtures. The sample was placed into a 1000-mL extraction cell, and a quantity of ZH-Oil (a kind of mixed aromatic hydrocarbons, whose carbon atoms range from $C_5$ to $C_{10}$) of about 150 mL was preintroduced into the filter. Once the sample was impregnated by the refluxing solvent, the valve of the tap funnel was subsequently closed, and the vacuum filtration began. The valve was opened after the tap funnel was filled, so the wax-laden solvent could flow into the flask. The procedure was repeated until the wax was completely stripped, which can be judged by observing whether wax crystals precipitate from the solvent in the tap funnel or not. At the end of the separation, anhydrous ethanol was used to rinse the catalyst particles several times and vacuum drying or drying with slight $N_2$ breezing was performed afterward (Figure 1c). In other case, the wax-free catalyst could be kept in the ethanol. The wax-free catalyst particles were submitted for PSD, SEM, EDS, and Brunauer−Emmett−Teller (BET) measurements.

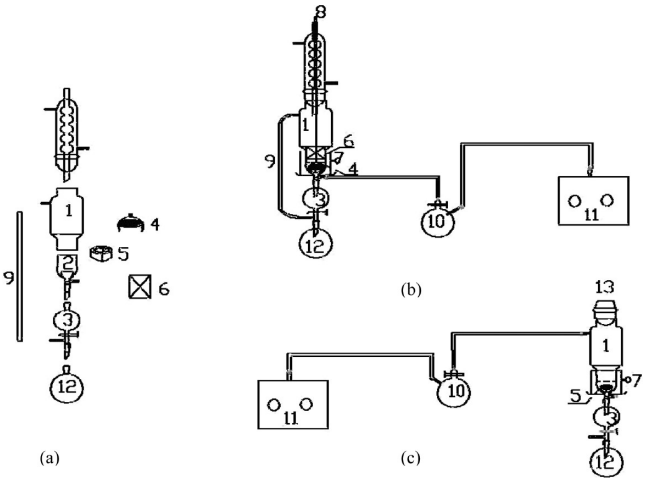


**Figure 1.** (a) Elements of EFS. (b) Schematic diagram of EFS. (c) Vacuum drying apparatus refitted from EFS. 1, Extraction cell; 2, filter; 3, tap funnel; 4, gas distributor; 5, porous PTFE lid; 6, wire mesh filter cartridge with variable mesh sizes; 7, columnar heating mantle; 8, pipeline of inert gas; 9, glass tube; 10, buffer; 11, vacuum pump; 12, flask; 13, plug.

**2.3. Catalyst Characterization.** *2.3.1. Particle Size Distribution (PSD).* The particle size distribution (PSD) of wax-free catalyst particles separated from wax/catalyst slurry mixtures was determined using a MALVERN Mastersizer 2000 laser particle size analyzer instrument, whose particle diameter detection ranges from 0.02 to 2000 $\mu$m. The details about particle size measurements and calculations can be found at the MALVERN Web site.[17] Multiple measurements (three to five) were made, and the average particle size was represented using the value of the volume moment. An ultrasonic bath was selected to better disperse the catalyst particles in distilled water or anhydrous ethanol. Our studies showed that the short application of ultrasound has a negligible impact on the particle distributions. The Mastersizer 2000 provides information on PSDs by volumetric ratio. The PSDs help to explain the attrition mechanisms: fracture (characterized by reduction in median particle size, $D_{50}$) and erosion (appearance of fine particles less than 5 or 10 $\mu$m).

*2.3.2. Brunauer−Emmett−Teller (BET) Surface Area and Pore Size Distribution.* The BET surface area, total pore volume, micropore volume, and average pore radius of the catalyst were calculated by the data of $N_2$ adsorption and desorption isotherms which were conducted on a Micromeritics ASAP 2010 automated system. All catalyst samples were degassed at room temperature for 2 h, at 373 K for 2 h, and then at 573 K for 4 h prior to each measurement.

*2.3.3. Particle Morphology.* Particle morphology was obtained using a Nova Nano SEM450 for each wax-free catalyst. Both fines and particles remaining in the chamber were analyzed using SEM.

*2.3.4. Elemental Distribution Analysis.* The catalyst samples prepared for SEM study were also used for particle surface element distribution analysis using energy-dispersive X-ray spectroscopy (EDS). EDS can provide information about the surface element distribution of different sections of individual catalysts.


dx.doi.org/10.1021/ie3014428 | Ind. Eng. Chem. Res. 2012, 51, 13123−13131

## 3. RESULT AND DISCUSSION

**3.1. Particle Size Distribution (PSD).** All the wax-free catalyst samples were measured with a MALVERN Mastersizer 2000 for PSDs. From the measurement results, one can obtain several average statistical parameters, which can be used to quantify any change in the average particle size of catalyst particles during the pilot-scale STSR Fischer−Tropsch synthesis (FTS). These include the following: (1) surface area moment mean diameter ($d_{3,2}$) or Sauter mean diameter (SMD)—the average diameter based on the unit surface area of a particle; (2) volume moment mean diameter ($d_{4,3}$)—the average diameter based on the unit volume of a particle; (3) $D_{10}$, $D_{50}$ (median), and $D_{90}$—the particle size when the cumulative size distribution reaches 10, 50, and 90%, respectively; (4) fraction of fine particles (particles less than 5, 10, and 20 $\mu$m in diameter); and (5) mode (the particle size corresponds to the high point of frequency curve). The Sauter mean diameter and volume moment diameter are calculated according to the following definitions:

$$d_{3,2} = \frac{\sum d_i^3 N_i}{\sum d_i^2 N_i} \qquad d_{4,3} = \frac{\sum d_i^4 N_i}{\sum d_i^3 N_i}$$

where $d_i$ is the particle diameter and $N_i$ is the number of particles of size $d_i$.

The reduction in Sauter mean diameter or volume moment diameter was expressed as the percentage of the initial value, i.e.

$$\Delta Y = \frac{Y(0) - Y(t)}{Y(0)} \cdot 100$$

The increase in the fraction of particles smaller than 5, 10, and 20 $\mu$m was calculated as

$$\Delta F = F(t) - F(0)$$

where $Y = d_{3,2}$ or $d_{4,3}$; $F$ represents a fraction of particles less than 5, 10, and 20 $\mu$m in diameter and $t$ is the time on stream; that is, $t$ = 0, 120, 216, 288, 312, 336, 360, and 408 h, respectively.

The PSDs in terms of relative volume frequency of different catalyst samples are shown in Figures 2−8, and Figure 9 gives the comparison results of the PSDs of these catalyst samples.

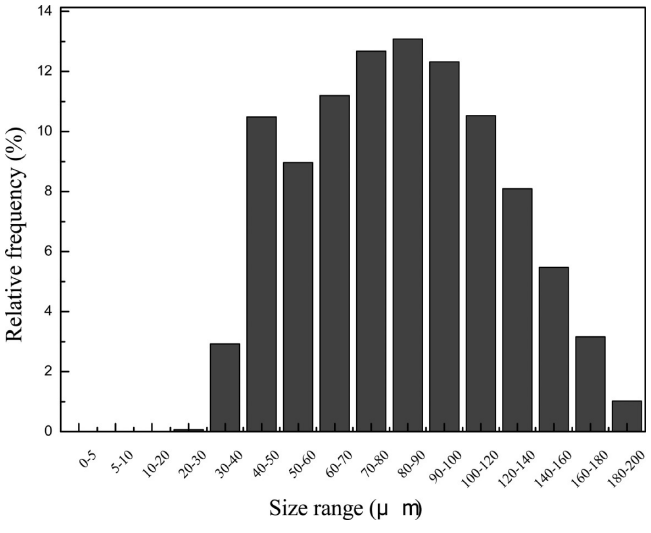


**Figure 2.** Relative PSD of an original iron catalyst.

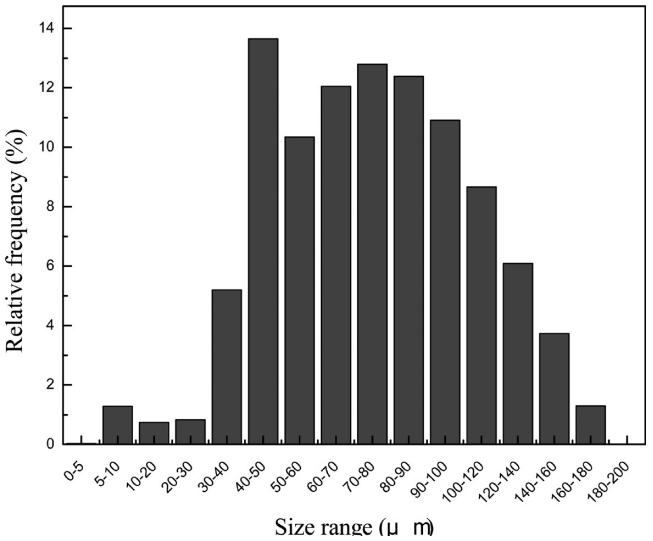


**Figure 3.** Relative PSD of an iron catalyst after 120 h F−T synthesis in the STSR.

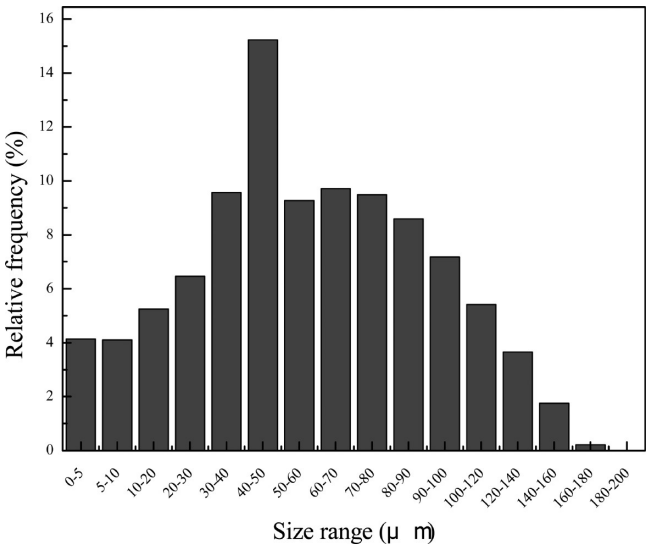


**Figure 4.** Relative PSD of an iron catalyst after 288 h F−T synthesis in the STSR.

The results of the PSD analysis are summarized in Tables 1 and 2, including the fraction of fine particles and values of $D_{10}$, $D_{50}$, $D_{90}$, $d_{3,2}$, $d_{4,3}$, $\Delta d_{3,2}$ (%), and $\Delta d_{4,3}$ (%).

It can be seen from Figure 9 that the entire PSD curve shifts toward smaller particles from that of the original catalyst samples with reaction time, indicating a significant continuous reduction in the mode value and an increase in the fine particles due to erosion/abrasion during the overall FTS. With regard to these samples, the PSD plot clearly indicates a bimodal distribution of particle size after FTS, which arises from the fracture of catalyst particles. The bimodal shifts to the right reveal that the large particles disintegrated into smaller fragments and simultaneously the disintegration of smaller fragments occurred.

The PSD of the original catalyst is shown in Figure 2. It is evident that the original catalyst particles present a unimodal distribution of particle size. The particle size varies from 20 to 200 $\mu$m, and the median value is 83 $\mu$m. After 120 h of F−T reaction, we see a handful of fine particles below 5 $\mu$m, and no


dx.doi.org/10.1021/ie3014428 | Ind. Eng. Chem. Res. 2012, 51, 13123−13131

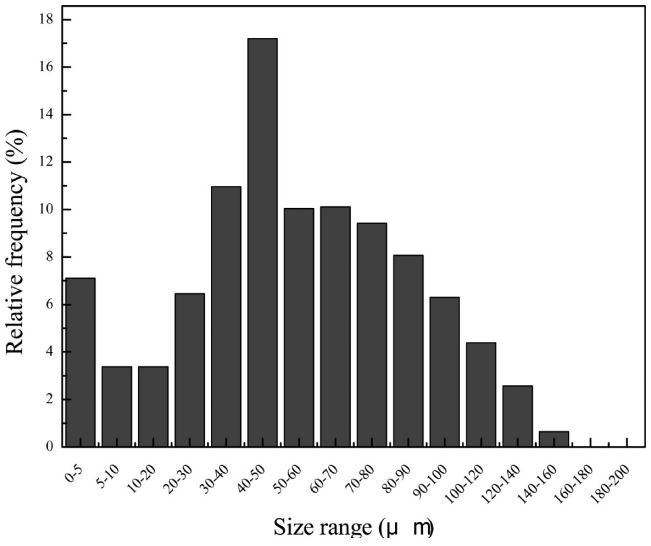


**Figure 5.** Relative PSD of an iron catalyst after 312 h F−T synthesis in the STSR.

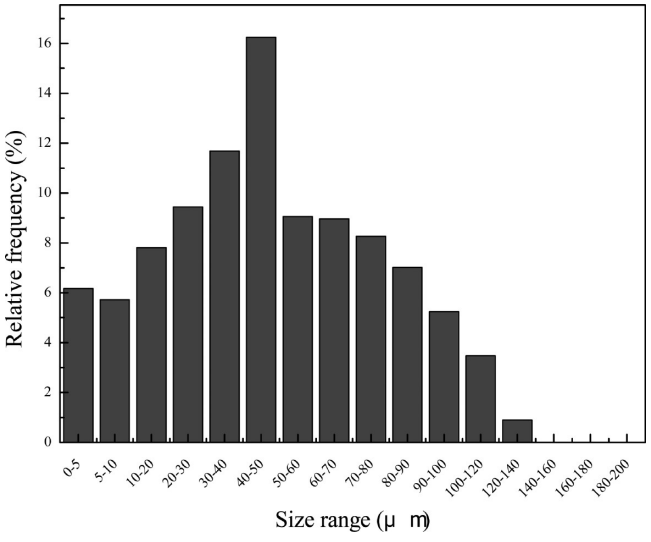


**Figure 6.** Relative PSD of an iron catalyst after 336 h F−T synthesis in the STSR.

particles larger than 180 $\mu$m in size can be found at the same time. Note that in the system existed 1.3% particles whose sizes ranged from 5 to 10 $\mu$m. With the synthesis time going on, the fine particles were becoming more and more numerous, whereas the larger particles became much less numerous. Also, the increase in the rate of the development of fine particles below 5 $\mu$m exceeded that of other particles. When the TOS reached 312 h, hardly any particles larger than160 $\mu$m could be detected, whereas the frequency of fine particles ($\leq$5 $\mu$m) was greater than 7%. At the end of the STSR test, there existed very few larger particles ($\geq$90 $\mu$m) and some of them may have been the agglomeration of smaller fragments. A larger bulk of catalyst particles had disintegrated into small fragments or chips. The results of Tables 1 and 2 confirm these findings. The fraction of fine particles smaller than 5 $\mu$m in diameter reached 18.25% after 408 h of FTS in the pilot-scale STSR, and particles smaller than 10 $\mu$m in diameter even reached up to 30.11%. The increase in fraction of ultrafine particles generated is a critical parameter for slurry phase reactor application. These

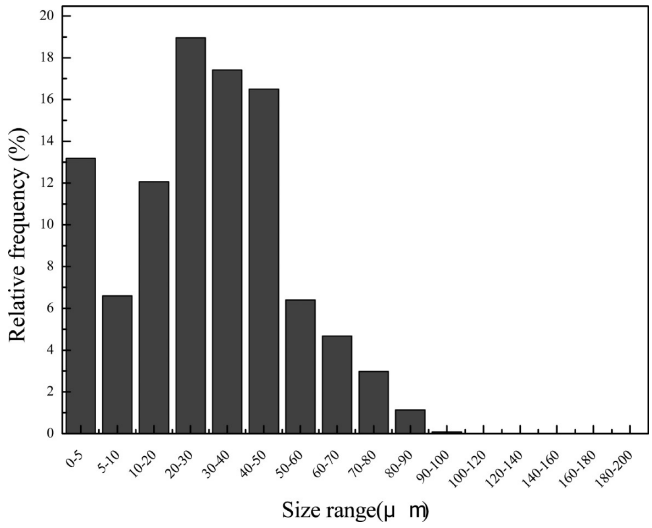


**Figure 7.** Relative PSD of an iron catalyst after 360 h F−T synthesis in the STSR.

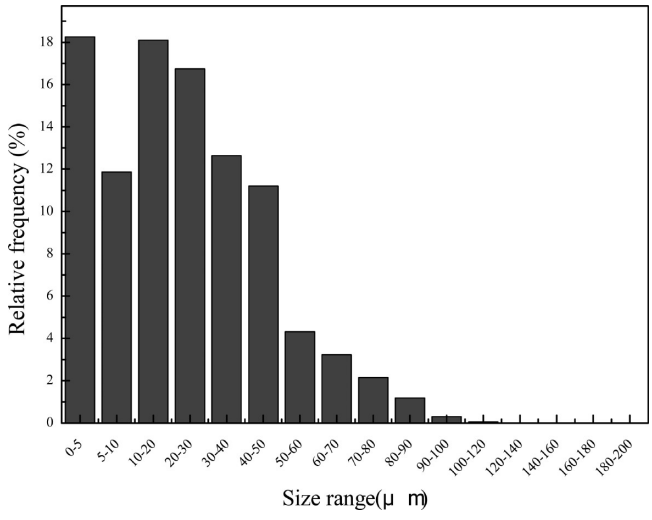


**Figure 8.** Relative PSD of an iron catalyst after 408 h F−T synthesis in the STSR.

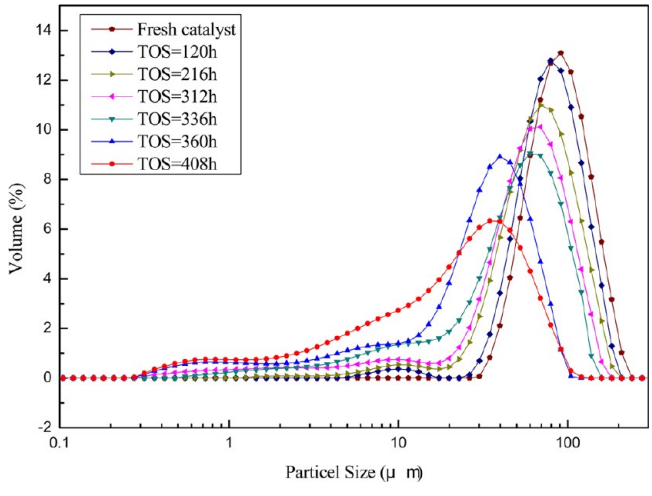


**Figure 9.** Volume frequency distribution of the catalyst sample collected at different times on stream during FTS in the STSR.


dx.doi.org/10.1021/ie3014428 | *Ind. Eng. Chem. Res.* 2012, 51, 13123−13131

**Table 1. Percent of Particles below 5, 10, and 20 μm Diameter during the STSR under Reactive Conditions[a]**

| | fraction of particles, % | | |
|---|---|---|---|
| t,[b] h | ≤5 μm | ≤10 μm | ≤20 μm |
| 0 | 0.00 | 0.00 | 0.00 |
| 120 | 0.03 | 1.32 | 2.06 |
| 216 | 1.03 | 3.08 | 5.29 |
| 288 | 4.14 | 8.23 | 13.48 |
| 312 | 7.10 | 10.48 | 13.85 |
| 336 | 6.17 | 11.89 | 19.70 |
| 360 | 13.19 | 19.78 | 31.85 |
| 408 | 18.25 | 30.11 | 48.21 |

[a]From volume distributions obtained using a Mastersizer 2000. [b]TOS, time on stream.

fines would cause difficulties in catalyst/wax separation, filters to plug, and product contamination. Based on the results in Table 2, the percent reductions in Sauter mean and volume moment diameters are severe for this iron catalyst used in STSR. We find that the value ranges from 0 to 93.45% for the Sauter mean diameter, and from 0 to 71.67% for the volume moment diameter with synthesis time. These values reflect mostly the size change in the larger particles due to fracture. The PSD plot also clearly revealed the fact that the changing of the mode value, to be specific, the value of the original catalyst was between 80 and 90 μm, then 40−50 μm for TOS = 120−336 h, then 20−30 μm when the TOS reached 336 h, and reduced to 10−20 μm at the end of the F−T run.

**3.2. Catalyst Morphology.** SEM was used to monitor the changes of catalyst morphology during the FTS. Spray-dried fresh catalysts are in the form of microspherical particles. The particle size distribution is rather broad, ranging from 30 to 200 μm in diameter.

SEM micrographs of these different time-on-stream catalyst samples separated from hydrocarbon wax are shown in Figures 10−13. In general, the catalyst particle fractured severely after reaction in STSR; fine particles are also seen obviously. The SEM results further confirm the accuracy of the PSD seen above.

As can be seen from Figure 10, for the catalyst sample withdrawn from the reactor at TOS = 120 h, a majority of grains are microspherical with smooth surfaces, which is similar to the as-received catalyst particles. Larger particles are around 100 μm, whereas smaller round ones are about 20 μm. However, attention should be paid to that some larger grains are irregularly shaped or, in other words, have sharp angular features due to the fracture of catalyst particles. The SEM

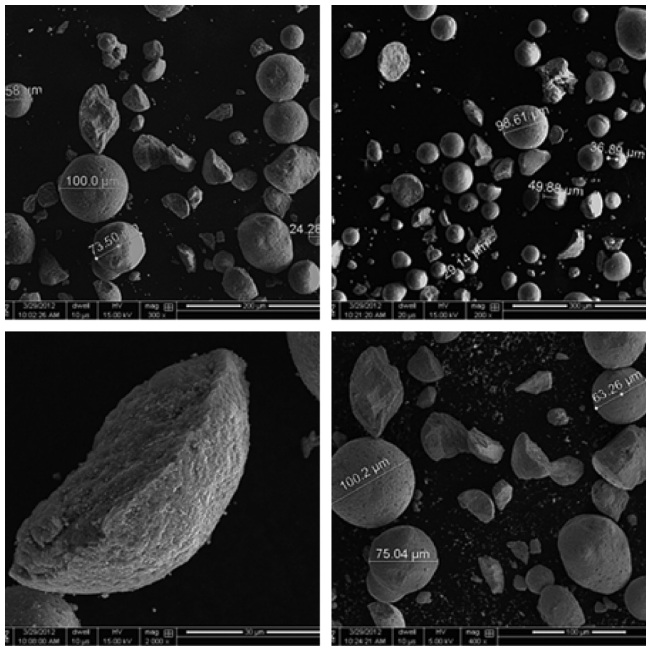


**Figure 10.** SEM images of spray-dried catalyst withdrawn from STSR after 120 h FTS (TOS = 120 h).

micrograph reveals that the particle morphology and size have slightly changed relative to the original catalysts according to the observation of very fine chips. Furthermore, small amounts of individual grains are not smooth but possess a round texture suggestive of the generation of fine particles due to abrasion. This is consistent with the PSD plot (Figure 3). Some of these small fragments are speculated to be caused by the blade of the STSR.

The SEM images of TOS = 288 h are shown in Figure 11. Similar to the PSD plot, the fine particles observed become more numerous, and the breakage of larger particles is apparent. It is easy to disintegrate these particles whose particle sizes are larger than 100 μm. The higher superficial area enhances their opportunities to collide with other particles or wall or blade and they have to bear more physical or chemical stress during the reaction.

Figure 12 gives SEM images of the same catalyst after 336 h of F−T reaction in STSR. It is apparent that the catalyst particle morphology has changed significantly. The bulk of the particles lost their sphericity, and the number of broken particles (fragments and chips) has increased. Some individual large particles, although possessing round texture, present rough external surfaces. Obvious fractures could be observed

**Table 2. Summary of Particle Size Distribution Measurement Results**

| t,[a] h | $D_{10}$[b] | $D_{50}$[b] | $D_{90}$[b] | $d_{3,2}$ | $d_{4,3}$ | $\Delta d_{3,2}$,[c] % | $\Delta d_{4,3}$,[d] % |
|---|---|---|---|---|---|---|---|
| 0 | 49.05 | 82.57 | 137.08 | 76.22 | 88.49 | – | – |
| 120 | 42.02 | 73.73 | 122.82 | 59.78 | 78.16 | 21.57 | 11.67 |
| 216 | 30.24 | 62.87 | 112.33 | 40.16 | 67.12 | 47.31 | 24.15 |
| 288 | 12.71 | 56.84 | 107.16 | 22.04 | 59.78 | 71.09 | 32.44 |
| 312 | 9.156 | 53.63 | 98.86 | 11.53 | 55.68 | 84.87 | 37.08 |
| 336 | 8.228 | 46.88 | 90.46 | 15.54 | 48.85 | 79.62 | 44.79 |
| 360 | 3.201 | 29.79 | 58.65 | 6.251 | 30.84 | 91.80 | 65.15 |
| 408 | 2.173 | 20.99 | 54.38 | 4.996 | 25.07 | 93.45 | 71.67 |

[a]TOS (time on stream), $t$ = 0, 120, 216, 288, 312, 336, 360, 408 h. [b]$D_i$, particle size when the percent cumulative size distribution reaches $i$; $i$ = 10, 50, 90, respectively. [c]$\Delta d_{3,2} = [(d_{3,2}(0) - d_{3,2}(t))/d_{3,2}(0)]\cdot 100$. [d]$\Delta d_{4,3} = [(d_{4,3}(0) - d_{4,3}(t))/d_{4,3}(0)]\cdot 100$.


dx.doi.org/10.1021/ie3014428 | Ind. Eng. Chem. Res. 2012, 51, 13123−13131

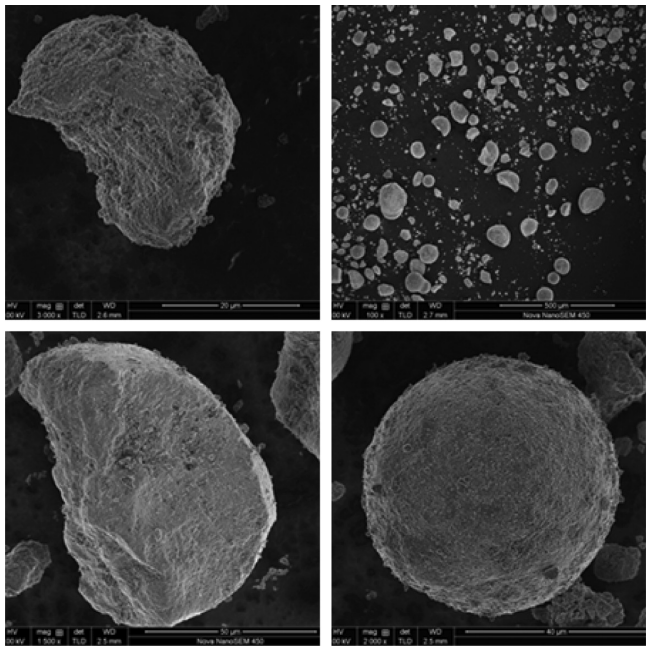

**Figure 11.** SEM images of spray-dried catalyst withdrawn from STSR after 288 h FTS (TOS = 288 h).

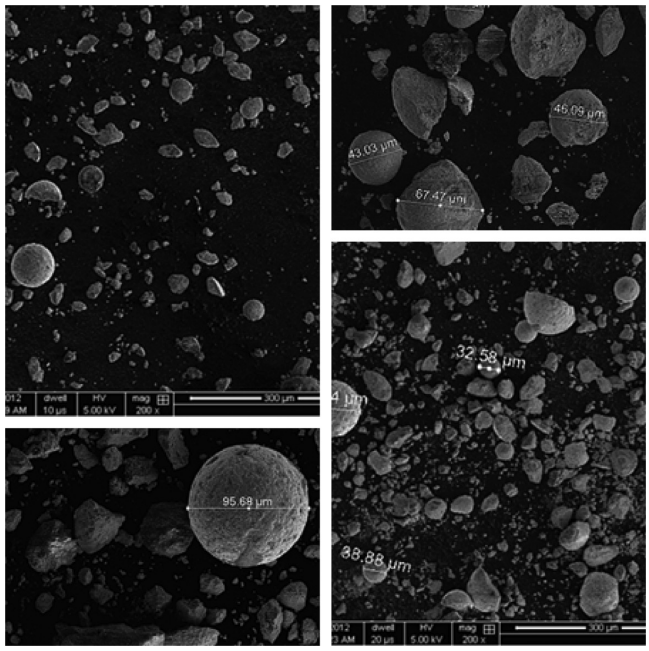


**Figure 12.** SEM images of spray-dried catalyst withdrawn from STSR after 336 h FTS (TOS = 336 h).

for these larger particles. Some smaller particles around 20−40 μm, however, still retain unchanged morphology (round and smooth surface). The presence of a significant number of particles smaller than 10 μm implies that this catalyst has undergone severe attrition.

From Figure 13, one can obtain that the particle morphology of this catalyst sample withdrawn at the end of the FTS (TOS = 408 h) has changed dramatically. There are hardly any larger spherical particles due to the disintegration into smaller fragments. Nearly all of particles have irregular external textures. Some visible large irregularly shaped grains representing agglomerates of smaller particles are likely due to the incomplete removal of hydrocarbon wax, but this does not affect the overall PSDs and the analysis of attrition by SEM images. Little residual wax on the catalyst can be removed by multiple washings with Zh-Oil. That the catalyst particles reduced significantly in size indicates the brittle strength of the fragments. These fragments caused by the fracture of larger particles exist with internal or surface flaws, and they become easy to fracture or abrade further. The reduction in particle size seen in the SEM images agrees well with the results from PSD measurement.

**3.3. Surface Element Analysis.** In order to gain further insight about the nature of catalyst attrition, SEM−EDXS was used to determine the composition of larger particles and fine particles, including the fracture section and spherical surface. The SEM images and element distributions of different sections/particles of three samples are shown in Figures 14−16 and Tables 3−5, among which Figures 14, 15, and 16 correspond to Tables 3, 4, and 5, respectively.

Figure 14 gives an SEM image of larger or fine particles, and Table 3 shows the weight ratios and atom ratios of Fe, Si, Cu, and K and the ratio of Fe/Si of the same section. One can obtain from Table 3 that the weight (or atom) ratio of Fe/Si for large particles (fracture section and spherical surface) at TOS = 120 h is not significantly different from that obtained from fine particles. However, for all of the round particles, the ratio of Fe/Si on the surface is relative greater than the fractures and fine particles. The same conclusion can be observed from Figures 15 and 16.

It also can be seen that after 288 h of F−T synthesis, the Fe/Si ratio of this catalyst is similar to that obtained from TOS = 120 h. However, this Fe/Si ratio obtained from TOS = 408 h is very different from that obtained from the previous two samples. Figure 16 tells the fact that these particles are all irregular fragments or fine particles, and Table 5 reveals that these particles possess a much smaller Fe/Si ratio.

The reason explaining this phenomenon is that volumetric change induced by phase transformation would cause chemical stress in the particles and further lead to attrition of iron carbides, which make it split off from the particles. Therefore, the chemical attrition accounts for a larger ratio than physical attrition in this Fe/Cu/K/$SiO_2$ F−T catalyst.

**3.4. Catalyst Particle Properties.** Catalyst particle properties were determined for three of the catalyst samples withdrawn on different times on stream, namely, TOS = 120, 288, and 408 h, respectively. The results from BET measurements are summarized in Table 6.

Table 6 clearly indicates that the total surface area reduced from 109.546 to 76.444 $m^2 \cdot g^{-1}$, whereas the average pore radius increased from 15.378 to 21.106 nm after the 408 h F−T run. The total pore volume remained almost unchanged within experimental error, which varied from 0.370 to 0.421 $cm^3 \cdot g^{-1}$. One should also notice that the micropore volume shows a trend to the smaller value. The BET surface areas have changed more obviously than the pore volume, and based on our experimental results, the change in total pore volume is small and negligible for this particular catalyst. Before the BET surface measurement, the catalyst had been treated with the removal of hydrocarbon wax from the inner and surface pores (extraction with organic solvent and degassed in high temperature), so any hydrocarbons that deposited in the particle pores can be considered to be essentially fully removed. Therefore, we suppose that the reduction in BET surface area and micropore volume are caused to a great extent by coke

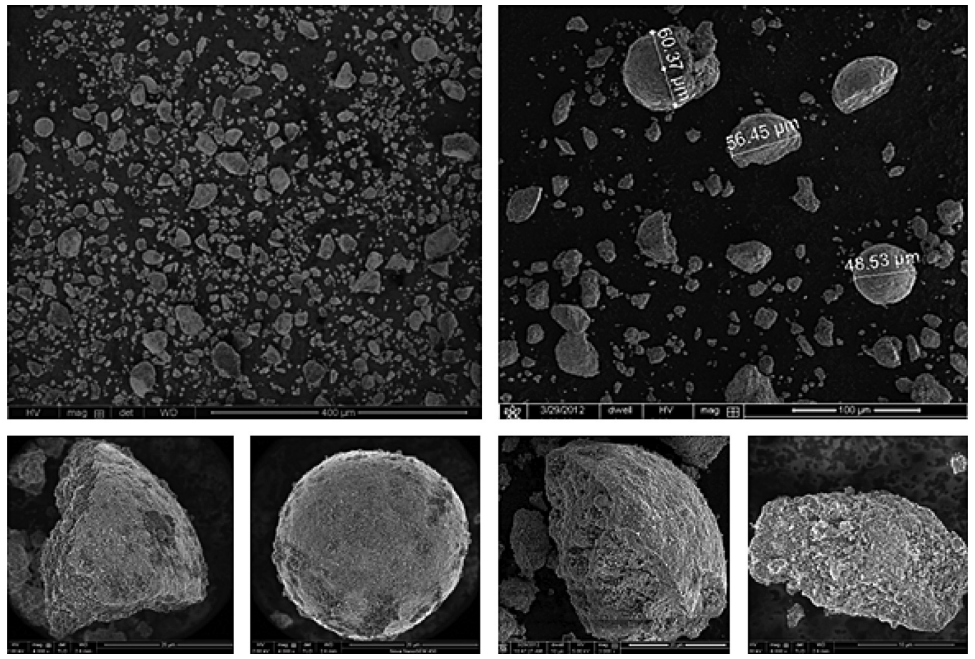


**Figure 13.** SEM images of spray-dried catalyst withdrawn from STSR after 408 h FTS (TOS = 408 h).

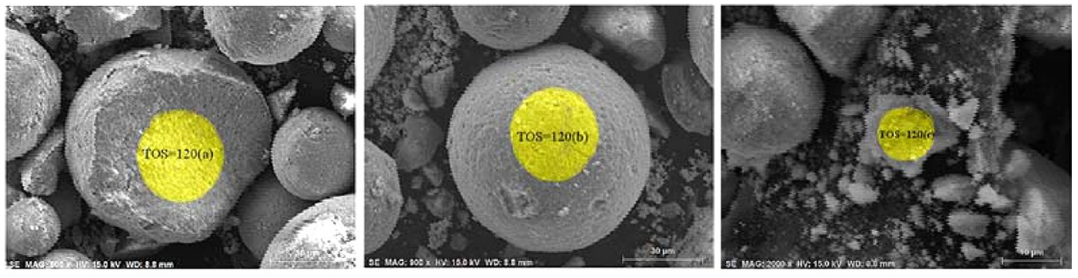


**Figure 14.** SEM images of different sections of catalyst after 120 h FTS (TOS = 120 h).

**Table 3. Element Distribution of Different Sections of a Catalyst When TOS = 120 h**

| | TOS = 120(a) | | TOS = 120(b) | | TOS = 120(c) | |
|---|---|---|---|---|---|---|
| element | wt % | atom % | wt % | atom % | wt % | atom % |
| Fe | 57.21 | 30.42 | 53.72 | 25.73 | 52.72 | 24.73 |
| Si | 5.97 | 6.32 | 4.77 | 4.54 | 4.85 | 4.52 |
| Cu | 3.84 | 1.79 | 1.75 | 0.74 | 1.63 | 0.67 |
| K | 1.81 | 1.38 | 1.54 | 1.05 | 1.42 | 0.95 |
| Fe/Si | 9.58 | 4.81 | 11.26 | 5.67 | 10.87 | 5.47 |

deposition. The collapse of pores and the fusion of micropores due to chemical force (for example, phase transformation leads to volume and pore radius changes) also account for these results.

On the basis of the above results and analysis, we know that this catalyst has undergone severe attrition, but these particle physical properties changed slightly, so it is hard to deduce the concrete relation between the attrition properties of the catalyst and the BET surface area and pore volumes.

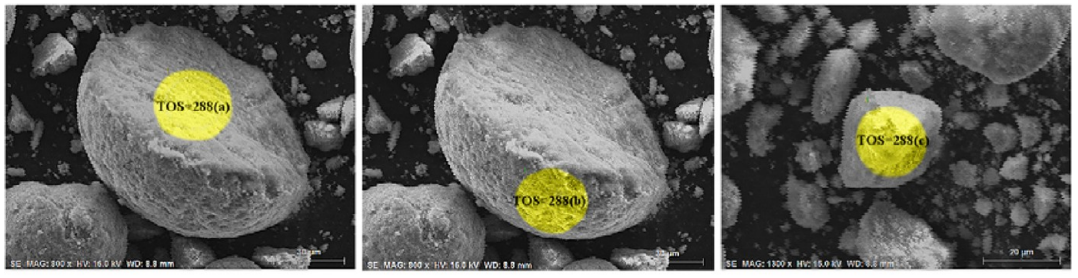


**Figure 15.** SEM images of different sections of catalyst after 288 h FTS (TOS = 288 h).


dx.doi.org/10.1021/ie3014428 | *Ind. Eng. Chem. Res.* 2012, 51, 13123−13131

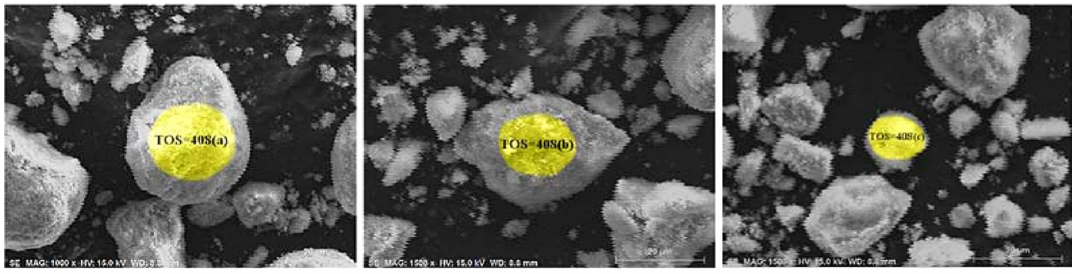


**Figure 16.** SEM images of different sections of catalyst after 408 h FTS (TOS = 408 h).

**Table 4. Element Distribution of Different Sections of a Catalyst When TOS = 288 h**

| | TOS = 288(a) | | TOS = 288(b) | | TOS = 288(c) | |
|---|---|---|---|---|---|---|
| element | wt % | atom % | wt % | atom % | wt % | atom % |
| Fe | 35.22 | 13.11 | 76.92 | 55.67 | 51.65 | 23.84 |
| Si | 3.36 | 2.48 | 6.28 | 9.04 | 4.72 | 4.33 |
| Cu | 2.91 | 0.95 | 4.39 | 2.79 | 3.35 | 1.36 |
| K | 0.73 | 0.39 | 1.83 | 1.90 | 1.26 | 0.83 |
| Fe/Si | 10.48 | 5.29 | 12.25 | 6.16 | 10.94 | 5.51 |

**Table 5. Element Distribution of Different Sections of a Catalyst When TOS = 408 h**

| | TOS = 408(a) | | TOS = 408(b) | | TOS = 408(c) | |
|---|---|---|---|---|---|---|
| element | wt % | atom % | wt % | atom % | wt % | atom % |
| Fe | 55.05 | 26.63 | 55.64 | 28.10 | 40.35 | 16.33 |
| Si | 5.78 | 5.56 | 7.71 | 7.74 | 7.00 | 5.63 |
| Cu | 2.15 | 0.91 | 2.85 | 1.26 | 1.76 | 0.63 |
| K | 1.40 | 0.97 | 1.46 | 1.05 | 1.31 | 0.76 |
| Fe/Si | 9.52 | 4.79 | 7.22 | 3.63 | 5.76 | 2.90 |

**Table 6. BET Surface Areas, Pore Volumes, and Pore Radii of the Iron Catalyst**

| sample | BET surf. area ($m^2 \cdot g^{-1}$) | micropore vol ($cm^3 \cdot g^{-1}$) | total pore vol ($cm^3 \cdot g^{-1}$) | av pore radius (nm) |
|---|---|---|---|---|
| TOS = 120 h | 109.546 | 0.0416 | 0.421 | 15.378 |
| TOS = 288 h | 94.640 | 0.0344 | 0.370 | 15.659 |
| TOS = 408 h | 76.444 | 0.0267 | 0.403 | 21.106 |

**3.5. Catalyst Attrition Behavior In STSR.** As speculated earlier in this paper, the catalyst attrition behavior in a pilot-scale STSR under reactive condition differs somewhat from that tested in the small-scale STSR or with other attrition test methods. Most of the published literature is confined to experimental tests; few studies relate to the attrition under pilot-scale reactors are reported, while our study explains this attrition behavior. Also, we would like to point out that the fines generated may be resulted from the fracture of smaller fragments caused by the disintegration of larger catalyst particles.

The original iron catalyst particles are round and of smooth sphericity. After different reaction times of F−T synthesis in the STSR, the catalysts have experienced largely reductions in mean particle size due to particle fracture and erosion/abrasion. The extent of attrition becomes more pronounced with synthesis time going on. The catalyst particle morphologies changed dramatically when the TOS reached 336 h. For the sample withdrawn at the end of the FTS, nearly all the catalysts have lost their original morphology, and large amounts of fine particles are visible. This is because of the breakup of larger particles and the breakup of smaller particles (including the original small particles and the chips) at the same time. It is well-known that the particles with pre-existing flaws/cracks are easy to disintegrate after they undergo a variety of stresses during reaction.

In order to evaluate and quantify the extent of attrition, many parameters are used in this study, but two different attrition parameters should receive more attention, namely, the increase of fine particles (ca. <5 or 10 $\mu$m) and the net change in the volume moment diameter or Sauter mean diameter. The first parameter commonly represents the index of abrasion/erosion, but in this study we prefer to describe it as the fracture of small fragments according to the SEM images observed. The second parameter represents the change of larger particles in size, and it is directly affected by the breakup of agglomerate and particles. Tables 1 and 2 show that this catalyst experienced a higher increase in the fine particles and reduction in the volume moment during the FTS. Not similar to other small-scale STSRs or SBCRs or other test methods, the catalyst in the pilot-scale STSR has to bear extreme impact and shear forces from the impeller blade. This rigorously hydrodynamic condition accompanied by the longer run duration makes the attrition more severe than the other literature reported.[11] Note that O'Brien et al.[18] reported a spray-dried and calcined Fe/Cu/K/$SiO_2$ catalyst with a spherical shape and size of 30−50 $\mu$m disintegrated to 1−3 $\mu$m particles during 24 h of FTS in an STSR under reactive conditions. Bukur et al.[7] studied the attrition strength of three iron catalysts made by adding different sources of silica (colloidal silica, tetraethyl orthosilicate, and potassium silicate). They found that the catalyst prepared employing colloidal silica had the highest attrition strength among all the supports tested, characterized by small nearly unchanged morphology, moderate erosion (fraction of fine particles smaller than 10 $\mu$m was 0.7%), and small extent of fracture ($D_{4,3}$ was 5.4%) after 345 h of testing in an STSR. Therefore, it is recognized generally that the sources, styles, concentration, network structure of $SiO_2$, and the addition way of silica play important roles in the improvement of the attrition resistance of iron catalyst used in the STSR. Of course, we also should realize that the nearly spherical and smooth shape is not sufficient to guarantee the high attrition strength of the catalyst; many factors mutually affect in the actual reaction.

When studying the attrition strength of spray-dried iron catalyst for slurry phase F−T synthesis, it is necessary to observe the effect of chemical attrition, which makes it hard to


dx.doi.org/10.1021/ie3014428 | Ind. Eng. Chem. Res. 2012, 51, 13123−13131

understand the attrition nature of iron catalyst due to the difficulties in monitoring and analyzing the specific phase composition. The purpose of our research is to study the attrition behavior (caused by physical and chemical attrition) of iron catalyst used in industrial-scale STSR or SBCR. In future work, we are going to examine the chemical causes of attrition in iron catalyst using SEM, EELS−STEM, TGA, XRD, XPS, and Mössbauer spectra, etc.

## 4. SUMMARY

The attrition properties of an iron catalyst were evaluated in a pilot-scale STSR under the F−T synthesis conditions. After 408 h of reaction, the particle size reduction due to fracture and erosion was severe. The observed reductions in the Sauter mean diameter and volume moment diameter was 93.45 and 71.67%, respectively. Also, the increase in the fraction of particles smaller than 10 $\mu$m was 30.11%. Spray drying and microspherical particles failed to maintain the higher attrition strength of this catalyst. In the pilot-scale STSR, the catalyst underwent severe attrition due to physical and chemical attrition, which makes a great deal of differences to the results obtained from experiment-scale tests or other attrition test methods. The attrition of this catalyst was mainly caused by fracture rather than erosion according to the SEM images.

SEM−EDS shows evidence that the generation of fine particles is caused in part by the breakage of larger or smaller particles; this woud also be led to by iron carbide segregation from the silica-containing region.

The BET surface area measurement indicates that the reduction in BET surface area and micropore volume and the increase in pore diameter may be caused by the coke and the fusion of micropores. It is hard to decide whether the changes of these physical properties have something to do with attrition or not.

In general, the pilot-scale STSR constitutes a more severe attrition behavior than other slurry phase reactor. Our studies mostly verify that the size change in the catalyst particles is due to fracture in the scale-up reactor. The current catalyst needs to be improved in attrition strength before it is considered for use in an industrial-scale rector. The nature of attrition phenomena is still not understood, and this arouses our interest in further studying the attrition of iron catalysts used in large-scale reactors by performing all kinds of characterization methods.

## ■ AUTHOR INFORMATION

### Corresponding Author

*E-mail: yyshi@ecust.edu.cn. Tel.: 021-64252274.

### Notes

The authors declare no competing financial interest.

## ■ ACKNOWLEDGMENTS

We acknowledge support from the State Key Laboratory of Chemical Engineering and the Research Center of Petroleum Processing of the East China University Of Science and Technology.

## ■ REFERENCES

(1) Zhao, R.; Goodwin, J. G., Jr.; Oukaci, R. Attrition assessment for slurry bubble column reactor catalysts. *Appl. Catal., A* **1999**, *189*, 99.

(2) Bhatt, B. L.; Schaub, E. S.; Hedorn, E. C.; Herron, D. M.; Studer, D. W.; Brown, D. M. In *Proceedings of Liquefaction Contractors Review Conference*; Stiegel, G. J., Srivastava, R. D., Eds.; U.S. Department of Energy: Pittsburgh, PA, 1992; p 403.

(3) Gulf Times (www.gulf-times.com); Oct 29, 2008.

(4) Zhou, C. W.; Lin, Q. The State of the Art Review of Fischer-Tropsch Synthesis Technology [J]. *Northwest Coal* **2010**, *8* (4), 93.

(5) Kalakkad, D. S.; Shroff, M. D.; Kohler, S.; et al. Attrition of precipitated iron Fischer- Tropsch catalysts. *Appl. Catal., A* **1995**, *133*, 335.

(6) Pham, H. N.; Nowicki, L.; Xu, J.; et al. Attrition Resistance of Supports for Iron Fischer-Tropsch Catalysts. *Ind. Eng. Chem. Res.* **2003**, *42*, 4001.

(7) Bukur, D. B.; Carreto-Vazquez, V. H.; Ma, W. P. Catalytic performance and attrition strength of spray-dried iron catalysts for slurry phase Fischer−Tropsch Synthesis. *Appl. Catal., A* **2010**, *388*, 240.

(8) Bukur, D. B.; Ma, W. P.; Carreto-Vazquez, V.; Nowicki, L.; Adeyiga, A. A. Attrition Resistance and Catalytic Performance of Spray-Dried Iron Fischer−Tropsch Catalysts in a Stirred-Tank Slurry Reactor. *Ind. Eng. Chem. Res.* **2004**, *43*, 1359.

(9) Adeyiga, A. A. *Development of Attrition Resistant Iron-Based Fischer−Tropsch Catalysts*; Prepared for the U.S. Department of Energy, Federal Energy Technology Center, Pittsburgh, PA, 15236, 2003.

(10) Pham, H. N.; Vierguta, A.; Gormley, R. J.; Datye, A. K. Improving the attrition resistance of slurry phase heterogeneous catalysts. *Powder Technol.* **2000**, *110*, 196.

(11) Bukur, D. B.; Ma, W. P.; Carreto-Vazquez, V. Attrition studies with precipitated iron Fischer−Tropsch catalysts under reaction conditions. *Top. Catal.* **2005**, *32*, 135.

(12) Bemrose, C. R.; Bridgwater, J. A review of attrition and attrition test methods. *Powder Technol.* **1987**, *49*, 97.

(13) Sarkar, A.; Seth, D.; Doziern, A. K.; Neathery, J. K.; et al. Fischer−Tropsch Synthesis: Morphology, Phase Transformation and Particle Size Growth of Nano-scale Particles. *Catal. Lett.* **2007**, *117*, 1.

(14) Zhao, R.; Goodwin, J. G.; Jothimurugesan, K.; Gangwal, S. K.; Spivey, J. J. Spray-Dried Iron Fischer−Tropsch Catalysts. 1. Effect of Structure on the Attrition Resistance of the Catalysts in the Calcined State. *Ind. Eng. Chem. Res.* **2001**, *40*, 1065.

(15) Zhao, R.; Goodwin, J. G.; Jothimurugesan, K.; Gangwal, S. K.; Spivey, J. J. Spray-Dried Iron Fischer−Tropsch Catalysts. 2. Effect of Carburization on Catalyst Attrition Resistance. *Ind. Eng. Chem. Res.* **2001**, *40*, 1320.

(16) Bukur, D. B.; Carreto-Vazquez, V.; Pham, H. N.; Datye, A. K. Attrition properties of precipitated iron Fischer−Tropsch catalysts. *Appl. Catal., A* **2004**, *266*, 41.

(17) http://www.malvern.com/.

(18) O'Brien, R. J.; Xu, L. G.; Bao, S. Q.; Raje, A.; Davis, B. H. Activity, selectivity and attrition characteristics of supported iron Fischer−Tropsch catalysts. *Appl. Catal., A* **2000**, *196*, 173.